

Article

# Direct Femtosecond Laser Fabrication of Superhydrophobic Aluminum Alloy Surfaces with Anti-icing Properties

Annalisa Volpe <sup>1,2,\*</sup>, Caterina Gaudio <sup>2</sup>, Leonardo Di Venere <sup>3</sup>, Francesco Licciulli <sup>3</sup>,  
Francesco Giordano <sup>1,3</sup> and Antonio Ancona <sup>2</sup>

<sup>1</sup> Dipartimento Interateneo di Fisica, Università degli Studi di Bari, Via G. Amendola 173, 70126 Bari, Italy; francesco.giordano@ba.infn.it

<sup>2</sup> Institute for Photonics and Nanotechnologies, CNR IFN, Via Amendola 173, 70126 Bari, Italy; caterina.gaudio@uniba.it (C.G.); antonio.ancona@uniba.it (A.A.)

<sup>3</sup> Istituto Nazionale di Fisica Nucleare-Sezione di Bari, via Orabona 4, 70125 Bari, Italy; leonardo.divenere@ba.infn.it (L.D.V.); francesco.licciulli@ba.infn.it (F.L.)

\* Correspondence: annalisa.volpe@uniba.it

Received: 30 May 2020; Accepted: 22 June 2020; Published: 24 June 2020



**Abstract:** Ice formation is a serious issue in many fields, from energy to aerospace, compromising the devices' efficiency and security. Superhydrophobicity has been demonstrated to be correlated to the anti-icing properties of surfaces. However, fabricating surfaces with robust water repellence properties also at subzero temperature is still a great challenge. In this work, femtosecond laser (fs-laser) texturing is exploited to produce superhydrophobic surfaces with anti-icing properties on Al2024, an aluminum alloy of great interest in cold environments, in particular for aircraft production. Our textured substrates present self-cleaning properties and robust water repellency at subzero temperatures. Moreover, outstanding anti-icing properties are achieved on the textured surfaces at  $-20\text{ }^{\circ}\text{C}$ , with water droplets bouncing off the surface before freezing.

**Keywords:** fs-laser; surface texturing; Al2024; anti-icing; wettability; superhydrophobicity

## 1. Introduction

Ice is a relevant problem in various industrial fields including transportation, energy and buildings. Ice accumulation can damage locks and dams [1], reduce the performance of cryogenic, refrigeration and air conditioning systems [2], cause power lines and telecommunication equipment outage [3]. Furthermore, ice accretions may result in dangerous road conditions and serious hazards during flights [4,5].

An ideal anti-icing surface should: (i) roll off the overcooled drops before they freeze [6] and (ii) induce a weak adhesion of the ice once it has accumulated [7,8]. Several studies have demonstrated that superhydrophobic surfaces (SHSs), i.e., surfaces with a water contact angle (CA) greater than  $150^{\circ}$  and a sliding angle (SA) less than  $10^{\circ}$  [9], in addition to the enhanced self-cleaning effect, have noteworthy anti-icing properties [6,10]. The methods proposed in the literature to produce superhydrophobic surfaces are mainly related to modifying the surface chemistry and/or topology. Wang et al. [11] produced several aluminum surfaces with various wettability from superhydrophilic to superhydrophobic by combining an etching method and a coating process. The authors found that also in overcooled condition (temperature  $T = -10\text{ }^{\circ}\text{C}$ , relative humidity  $RH = 90\%$ ), water droplets bounced before freezing, despite the increase of the SA (from  $1^{\circ}$  to  $22^{\circ}$ ). The authors also found a reduction of the ice adhesion with respect to the untreated surface and durability of this behavior up to 20 ice/deicing processes.

Significant progress has been made in the fabrication of superhydrophobic surfaces on metallic substrates reproducing the micro-nano structures inspired by the topography of the lotus leaf [12]. In particular, laser surface texturing is gaining extensive interest and produces various well-controlled microstructures on metallic surfaces [13]. During the ablation process, the material is removed from the substrate and the features created depend on the laser parameters, such as the pulse duration, the laser fluence and the repetition rate. The wetting properties of nanosecond laser-fabricated superhydrophobic aluminum surfaces were studied by Jagdheesh et al. [14]. Superhydrophobicity has also been achieved on metal surfaces with a two-step ns-laser texturing process [15] or combining short-pulsed laser ablation with subsequent treatment in chlorosilane [16].

Recently, great attention has been paid to the use of ultrashort laser sources for the functionalization of surfaces. Ultrafast laser sources can fabricate nano/microscale surface structures on a wide range of materials from metals [17,18] to dielectrics [19,20], with an almost negligible thermal load to the substrate as compared to nanosecond lasers. The ultrashort laser fabrication of SHS has been reported on several metallic substrates, such as Al7075 [21], and stainless steel [22]. The fabrication of metallic SHS combining direct laser writing and direct laser interference patterning has also been reported [23,24].

Only a few of the research papers found in the literature on the direct ultrashort laser fabrication of metallic superhydrophobic surfaces delve into their anti-icing properties. In general, these works focus on the delay in the droplets freezing time [22,25], without discussing other issues related to the ice formation, such as the easy removal of impurities that can accelerate the ice nucleation and the robustness of the wetting behavior. Another important issue is the freezing of water dripping on cold substrates, such as in heat transfer surfaces, where ice accretion could result in poor device efficiency.

In this paper, we report a study on the fabrication and characterization of superhydrophobic surfaces on flat Al2024 with self-cleaning and robust anti-icing properties. Aluminum alloys are widely used for outdoor structures, such as ground wires and phase conductors of overhead power lines, as well as aircrafts wings and fuselage, which can be subjected to ice accretion. We use a one-step direct fs-laser ablation technique without any chemical post-treatment. The wetting properties of the surfaces and their robustness at subzero temperatures have been explored, showing a stable wetting at subzero temperature. The laser-fabricated superhydrophobic surfaces exhibit both excellent self-cleaning and anti-icing performances, representing a promising strategy for ice protection in many applications in cold environments.

## 2. Experimental Section

Flat Al2024 sheets with a thickness of 1 mm were used as substrates. The samples were washed with isopropyl alcohol in an ultrasound bath for 10 min and then processed with an ultrafast solid-state laser system (mod. TruMicro Femto Ed. From Trumpf GmbH, Ditzingen, Germany) based on the chirped pulse amplification technique (CPA). Such laser source emits at a wavelength of 1030 nm and provides an almost diffraction-limited beam ( $M^2 < 1.3$ ) linearly polarized with a pulse duration of 900 fs.

The beam has been moved over the sample through a galvo-scan head (IntelliSCAN 14, SCAN-LAB, Puchheim, Germany), equipped with a 100 mm telecentric lens which focused the beam with a spot size  $d$  of about 20  $\mu\text{m}$ .

The parameters used for the micromachined process are listed in Table 1. Each laser texturing test was performed overlapping two perpendicular scanning patterns, in order to generate periodic square-shaped structures, as previously reported in other studies [22,26]. The distance between consecutive scanning lines, indicated as hatch distance in Table 1, was varied in a wide range from 10 to 500  $\mu\text{m}$ . From the scanning speed  $v$  and the laser repetition rate, the pulses per spot can be calculated as:

$$pps = d \times \frac{f}{v} = 40 \quad (1)$$

**Table 1.** Process parameters for the microstructuring of the Al2024 via laser ablation.

Pulse Energy ( $\mu\text{J}$ )	Repetition Rate $f$ (kHz)	Scan Seed $v$ (mm/s)	Hatch Distance $h$ ( $\mu\text{m}$ )
12.2	100	50	10, 50, 100, 200, 500

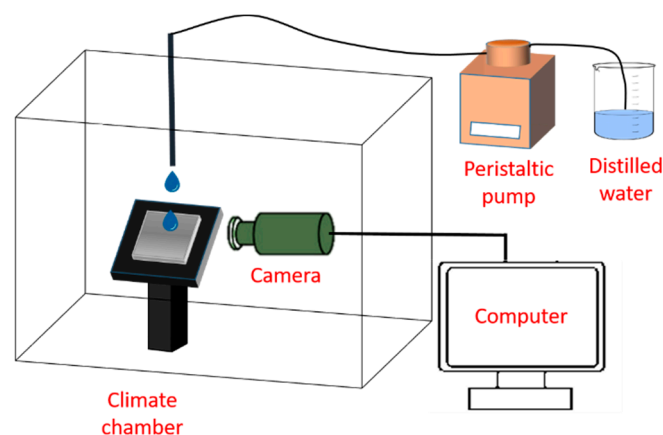
Each micromachining was carried out in ambient air on a target area of  $1 \times 1 \text{ mm}^2$  or  $2 \times 2 \text{ mm}^2$ , depending on the test to be performed. After fs-laser texturing the samples were stored in air with no further cleaning procedures.

The topography of the surface structures was characterized using a scanning electron microscope (SEM, Carl Zeiss mod. Sigma, Oberkochen, Germany).

Thermal aging of the samples was performed in a climate chamber (Temperature Test Chambers-ACS DY16T) at  $70 \text{ }^\circ\text{C}$  for 15 h. The climate chamber temperature can range from  $-30$  to  $130 \text{ }^\circ\text{C}$ , so the same chamber was used for the test at subzero temperatures, too.

Static contact angle (CA) measurements were conducted using a digital goniometer, consisting of a Dino-lite portable microscope combined with a cold light lamp for back-lighting of the drop. Drops of distilled water of  $10 \text{ }\mu\text{L}$  in volume were gently placed on the surface with a micropipette. The CA measurements were performed in a range from ambient temperature (approximately equal to  $20 \text{ }^\circ\text{C}$ ) to  $-20 \text{ }^\circ\text{C}$  in the climate chamber. An average of three CA measurements at various points of the laser-patterned region was reported. Before each water droplet deposition, the sample was kept 15 min in the climate chamber to thermalize with it. The ambient humidity was constantly monitored.

The self-cleaning property was evaluated by recording the removal of particles of different sizes spread on the substrate. The sample was fixed on the holder inclined at  $10^\circ$  by using double-sided adhesive. The  $10 \text{ }\mu\text{L}$  deionized water drops were continuously and uniformly dropped thanks to a peristaltic pump Minipuls 3 (Gilson, Middleton, WI, USA) at a rate of 1 drop/s from a height of about 1.5 cm on the sample covered of particles of different grain dimensions (from some tens of micrometers to 1 mm). Water droplets impact and rolling off were recorded using a high-speed camera (CR5000x2, Optronis, Kehl, Germany) at a frame rate of 500 fps. All self-cleaning experiments were performed at a temperature of about  $20 \text{ }^\circ\text{C}$ . Similarly, the anti-icing tests were carried out through water dripping at a rate of 2 drops/s, but putting the tilted sample in the climate chamber at  $-20 \text{ }^\circ\text{C}$ , as presented schematically in Figure 1. The experiment was recorded using the Dino-PLUS camera because the high-speed camera was too large to be placed into the climate chamber.

**Figure 1.** Schematic of the water dripping test performed in the climate chamber at  $-20 \text{ }^\circ\text{C}$ .

### 3. Results and Discussion

Regular microgrid structures with a groove of about  $8 \text{ }\mu\text{m}$  depth have been textured on the Al2024 sample by scanning the surface in two perpendicular directions. Figure 2 shows the SEM images of the laser-textured surfaces at increasing hatch distance from 10 to  $500 \text{ }\mu\text{m}$ . The surface in Figure 2a does not

look as uniform as the surfaces in Figure 2c–f. This can be even better highlighted in Figure 2b, where a magnification of the laser track is reported. In this case, the hatch distance is smaller than the laser spot size. Therefore, in addition to the succession of valleys and peaks of the hatch geometry, a stronger laser ablation generating a rough micro-nanostructure was noticeable. For larger hatches, weaker ablation was experienced, thus making the final laser-generated micro-nano structures more uniform.

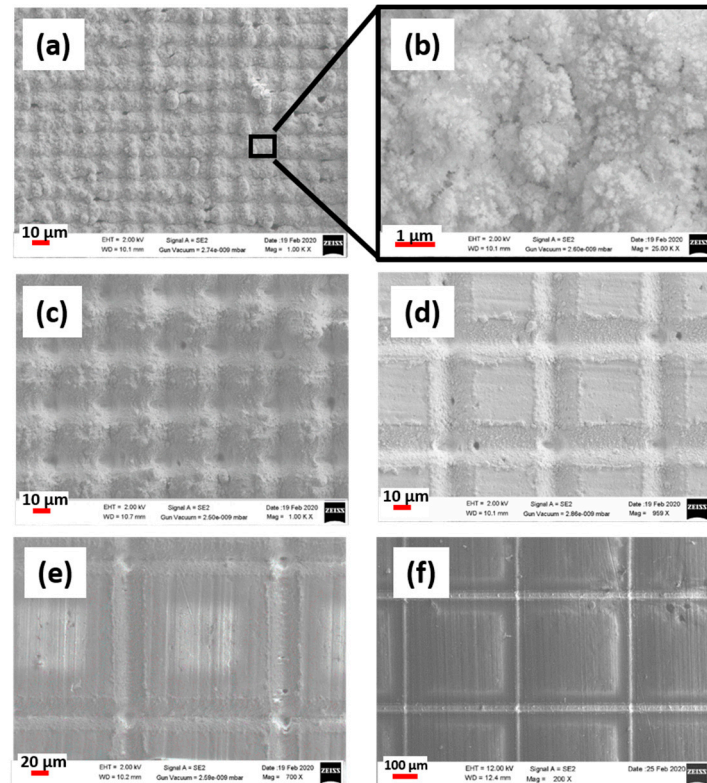


**Figure 2.** SEM pictures of laser-textured surfaces. The hatch distance between consecutive scanning lines are: (a,b) 10  $\mu\text{m}$  (two different magnifications), (c) 50  $\mu\text{m}$ , (d) 100  $\mu\text{m}$ , (e) 200  $\mu\text{m}$  and (f) 500  $\mu\text{m}$ .

Just after the laser treatment, all the surfaces were highly hydrophilic, with an instantaneous spread of the drop once it touched the surface. Therefore, no  $CA$  was measured. This was ascribed to hydrophilic metal oxides compounds formed on the surface after patterning, as reported by Quère et al. [27], that make the freshly laser-treated samples behave as a 3D porous medium. However, after the thermal aging process, the textured surfaces showed a hydrophobic behavior, which can be explained by a change in surface chemistry [28]. X-ray photoelectron spectroscopy (XPS) measurements carried out by Cardoso et al. [29] on Al2024 surfaces textured with similar laser process conditions, correlate the superhydrophobicity achieved after the aging process to the higher concentration of carbon organic molecules responsible for low surface energy. Conversely, the freshly treated surface was enriched with fresh aluminum oxides that are highly hydrophilic. The authors ascribed the change in wettability to the chemisorption of organic molecules present in the ambient air by the surface aluminum oxides. It was thus confirmed that, in this specific case, surface chemistry has a greater influence than topography on the wettability of a laser-textured surface. Similar conclusions have been reached also on other fs-laser-textured metals, such as stainless steel [30].

The effect of different microgrid spacing on surface wettability was investigated and compared to the pristine sample, which presents hydrophilicity with contact angle slightly above 80° (Figure 3a). The static contact angle measurements for all the textured samples with  $h \leq 200 \mu\text{m}$  showed a superhydrophobic behavior. Figure 3b shows the exemplary case of  $h = 50 \mu\text{m}$ , which had exactly the same wetting behavior of all the other SH samples. The droplet, gently placed on the surface, did not remain attached to it but could be moved right and left dragged by the micropipette (Figure 3c,d), still

maintaining its original shape even if pressed. When released, the droplet bounced off, making the CA measurement not possible. When such behavior occurs, it is commonly assumed that the CA is equal to  $180^\circ$  [31]. After a few hours of thermal aging, the surface energy of the laser-patterned region is very low [14]. The bouncing of the water droplet is attributed to the presence of air between the droplet and the solid surface. The air, confined within the laser-patterned structures, acts as a cushion and reduces the direct solid–liquid interaction, as explained by the Cassie–Baxter model [32].

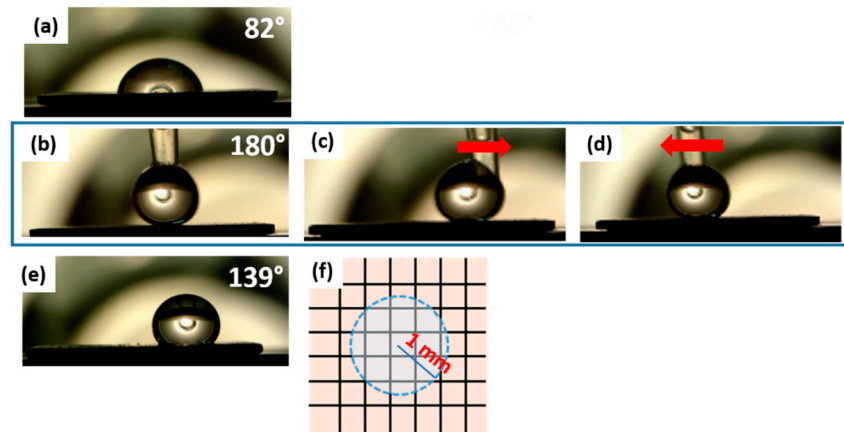


**Figure 3.** Images of the  $10\ \mu\text{L}$  droplet deposited on (a) the pristine surface and on (b) the laser-textured surfaces ( $h = 50\ \mu\text{m}$ ). The snapshots show the dynamic of the droplet, which can be moved right (c) and left (d). (e) A  $10\ \mu\text{L}$  droplet on the textured surface  $h = 500\ \mu\text{m}$  with (f) the schematic upper view, the blue dotted line represents the contour of the droplet and is in touch with the textured material.

Figure 3e shows the droplet deposited on the laser surface textured with  $h = 500\ \mu\text{m}$ . Here, the microstructured surface presents hydrophobicity with CA  $139^\circ$ . Therefore, at such a large hatch distance the superhydrophobicity obtained for denser microgrid structures is lost. This behavior can be attributed to the reduced portion of the micromachined surface that came into contact with the droplet in favor of the hydrophilic nonpatterned area, located in the center of the microcells [29]. Indeed, considering that the laser groove is typically  $20\ \mu\text{m}$  wide and the drop-surface contact area has a radius of  $1\ \text{mm}$ , only about 15% of the droplet surface gets in touch with the laser modified region when  $h = 500\ \mu\text{m}$  (Figure 3f). Consequently, the trapped air is not enough to sustain the droplet weight.

The laser-textured SHS, namely samples with ( $h \leq 200\ \mu\text{m}$ ), exhibited self-cleaning performances. In Figure 4, different time frames of a droplet rolling off the  $10^\circ$  tilted surface previously coated with a layer of grains of different sizes have been reported. The water droplet rolling under its own gravity formed a liquid bridge among the neighboring contaminant particles realizing in such a way a cluster that moves away from the surface, leaving the aluminum surface clean and dry.

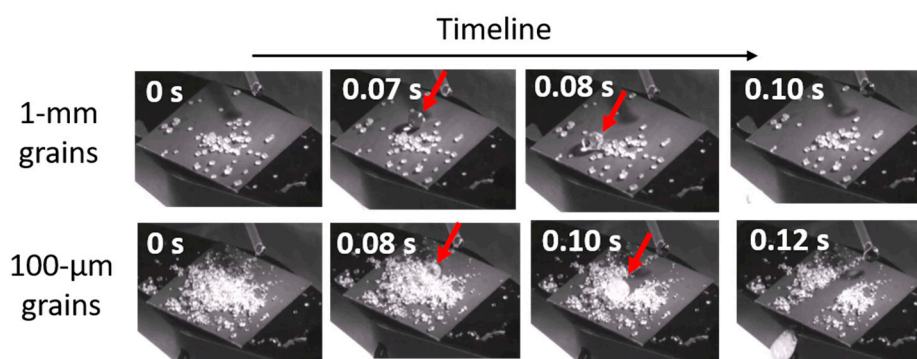


**Figure 4.** Self-cleaning property of the laser-textured aluminum substrate. Snapshot of the droplet rebounding. Two different grain dimensions have been tested.

The property of easily removing deposited contaminant particles can be very useful to obtain a surface with enhanced anti-icing properties. Indeed, the presence of impurities was demonstrated to accelerate ice nucleation [33].

One of the main issues which may prevent SHS from having anti-icing properties is that the CA usually decreases when the surface is exposed to overcooled conditions, therefore losing its superhydrophobicity [34]. In our case, the robustness of the wetting behavior of the laser-treated sample was evaluated by recording the water contact angle on textured  $h = 50 \mu\text{m}$  and untextured surfaces at different ambient temperatures below zero. In Figure 5, laser-textured and untextured surfaces are compared at different subzero temperatures. Starting from  $0^\circ\text{C}$ , the textured surface lost the original superhydrophobicity, but maintained hydrophobicity in the range of temperature between  $0$  and  $-20^\circ\text{C}$ . On average, both surfaces had a similar decrease in the CA (Figure 5) with temperature. This behavior can be associated with water condensation on the surface at low temperatures and high humidity [34]. However, such a decrease was more pronounced for the textured surface, which registers an almost double slope with respect to the pristine surface. Indeed, the air trapped in microstructures was easily substituted by water under high  $RH$ , causing the more pronounced decrease in CA values.

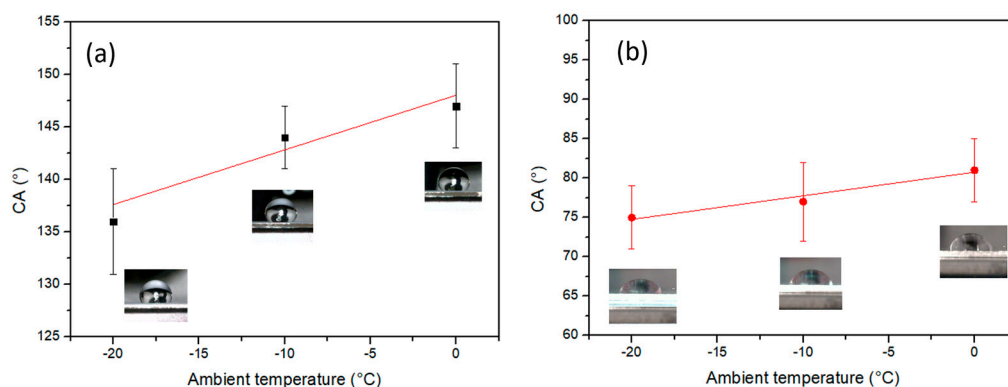


**Figure 5.** Evolution of the contact angle (CA) with the ambient temperature. The  $10 \mu\text{L}$  drops were gently deposited on (a) the micromachined sample ( $h = 50 \mu\text{m}$ ), black square) and (b) on the pristine one (red circle).

The robustness of the surface hydrophobicity at a subzero environment was tested freezing the droplet at  $-20^\circ\text{C}$  and then returning to  $20^\circ\text{C}$  in a controlled manner. On both surfaces, at  $-20^\circ\text{C}$ , a protrusion appeared on top of the frozen droplet conferring a peach shape, which can be attributed to the specific volume difference between ice and water [35]. However, as the surface returned to  $20^\circ\text{C}$ , the reference droplet on the textured surface resumed its original shape and CA value before solidification. In particular, the droplet appeared to be resting upwards and the discontinuous three-phase contact line between the drop and surface was basically recovered, which was similar to the original contact state (Figure 6a). The observations above indicate the robust hydrophobic properties of the surface, which can promote a stable anti-icing behavior, even after many thermal cycles. Conversely, as emerged from Figure 6b, the reference drop collapsed on the untextured surface completely wetting it and generating, after a further lowering of temperatures, an unruly layer of ice. In a real device, this uncontrolled water layer, penetrating the equipment and freezing, may result in the accretion of a wild ice layer which can cause severe damages to the equipment due to its volume expansion.

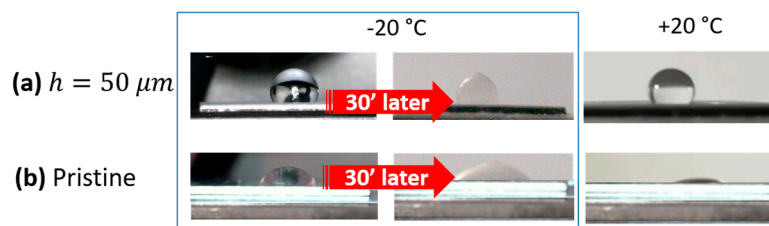


**Figure 6.** Droplet evolution after a thermal cycle. The 10  $\mu\text{L}$  drop, gently set (a) on the micromachined sample ( $h = 50 \mu\text{m}$ ), is compared with the droplet (b) on the pristine one.

Ultimately, the dynamic anti-icing performance of the textured samples was investigated comparing the ice formation on a machined sample ( $h = 50 \mu\text{m}$ ) and on the unprocessed one. The water droplets were continuously and uniformly dropped from a height of about 1.5 cm on the samples stored at  $-20 \text{ }^\circ\text{C}$ . Figure 7 displays the comparative results during and after the test. After 3 min, the untreated surface was covered with ice, while no frozen spot could be observed on the textured surface. This can be attributed to different water adhesion properties. When a droplet fell onto the untreated Al2024, it remained and expanded on the surface due to the hydrophilic nature of the material, thus freezing after a while (Figure 7a). In contrast, thanks to the stable water repellent behavior of the textured surfaces even in a subzero environment (see Figure 7b), the drop bounced off the textured surface very quickly, thus making the drop freezing and an ice layer accretion very unlikely.

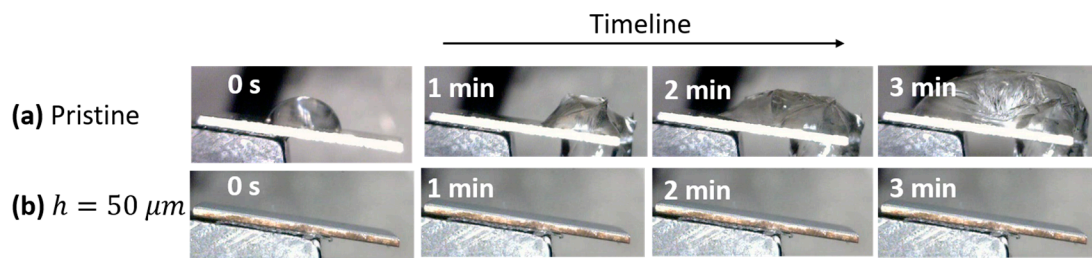


**Figure 7.** Time evolution of water accumulation (a) on the pristine surface compared with (b) the laser-treated Al2024 one (at  $-20 \text{ }^\circ\text{C}$ ).

#### 4. Conclusions

We proposed a one-step fs-laser microprocessing method to obtain superhydrophobic Al2024 surfaces with robust water repellent behavior and anti-icing properties.

Microgrid structures with different spacing were textured by direct fs-laser writing. The microgrid spacing  $h$  was shown to have a great influence on the wetting behavior of the surfaces. In particular, below a certain hatch spacing value ( $h \leq 200 \mu\text{m}$ ) superhydrophobicity has been reported. On these samples, the self-cleaning behavior with contaminant particles of different sizes was successfully demonstrated. This property can help in delaying the ice formation, being any deposited particle a natural ice nucleation accelerator.

The hydrophobic behavior of the textured surfaces was proved also at subzero temperature, showing that this remained unchanged even after a thermal cycle. Namely, the droplets deposited on the textured substrate recovered their original shape, thus completely preventing the surface to be wetted, as it conversely happened on the pristine sample. In this last case, the water froze at subzero temperatures and created an uncontrolled layer of ice.

Moreover, the fs-laser-textured surfaces showed a dynamic anti-icing performance even in a very low-temperature environment ( $-20 \text{ }^\circ\text{C}$ ). In particular, our tests proved that the laser-fabricated microstructures on the Al2024 surface favor effective anti-icing because of the stable water repellent properties that are preserved even at subzero temperatures, thus inhibiting water adhesion and preventing ice formation.

**Author Contributions:** Conceptualization, A.V.; methodology, A.V., C.G. and L.D.V.; software, L.D.V. and F.L.; investigation, A.V., L.D.V. and F.L.; data curation, A.V.; writing—original draft preparation, A.V.; writing—review and editing, all authors; supervision, F.G. and A.A.; funding acquisition, A.A. All authors have read and agreed to the published version of the manuscript.

**Funding:** This research was funded by the Italian Ministry of Education, University and Research (MIUR) within the Project AIM184902B-1-ATT1.

**Acknowledgments:** The authors gratefully acknowledge the G. Palumbo for the provision of the Al2024 samples and Pietro Paolo Calabrese for his technical support.

**Conflicts of Interest:** The authors declare no conflicts of interest. The funders had no role in the design of the study; in the collection, analyses, or interpretation of data; in the writing of the manuscript, or in the decision to publish the results.

## References

1. Frankenstein, S.; Tuthill, A.M. Ice adhesion to locks and dams: Past work; future directions? *J. Cold Reg. Eng.* **2002**, *16*, 83–96. [[CrossRef](#)]
2. Irigorry, J.; Tao, Y.X.; Jia, S. A critical review of properties and models for frost formation analysis. *HVAC&R Res.* **2004**, *10*, 393–420.
3. Laforte, J.L.; Allaire, M.A.; Laflamme, J. State-of-the-art on power line de-icing. *Atmos. Res.* **1998**, *46*, 143–158. [[CrossRef](#)]
4. Lynch, F.T.; Khodadoust, A. Effects of ice accretions on aircraft aerodynamics. *Prog. Aerosp. Sci.* **2001**, *37*, 669–767. [[CrossRef](#)]
5. Vercillo, V.; Karpen, N.; Laroche, A.; Guillén, J.A.M.; Tonnichia, S.; Jorge, R.d.A.; Bonaccorso, E. Analysis and modelling of icing of air intake protection grids of aircraft engines. *Cold Reg. Sci. Technol.* **2019**, *160*, 265–272. [[CrossRef](#)]
6. Mishchenko, L.; Hatton, B.; Bahadur, V.; Taylor, J.A.; Krupenkin, T.; Aizenberg, J. Design of ice-free nanostructured impacting water droplets. *ACS Nano* **2010**, *4*, 7699–7707. [[CrossRef](#)]
7. Wang, Y.; Xue, J.; Wang, Q.; Chen, Q.; Ding, J. Verification of icephobic/anti-icing properties of a superhydrophobic surface. *Appl. Mater. Interfaces* **2013**, *5*, 3370–3381. [[CrossRef](#)] [[PubMed](#)]
8. Kulinich, S.A.; Farzaneh, M. Ice adhesion on super-hydrophobic surfaces. *Appl. Surf. Sci.* **2009**, *255*, 8153–8157. [[CrossRef](#)]
9. Guo, Z.; Liu, W.; Su, B. Journal of colloid and interface science superhydrophobic surfaces: From natural to biomimetic to functional. *J. Colloid Interface Sci.* **2011**, *353*, 335–355. [[CrossRef](#)] [[PubMed](#)]
10. Jamil, M.I.; Ali, A.; Haq, F.; Zhang, Q.; Zhan, X.; Chen, F.; Jamil, M.I.; Ali, A.; Haq, F.; Zhang, Q.; et al. Icephobic strategies and materials with superwettability: Design principles and mechanism. *Langmuir* **2018**, *34*, 15425–15444. [[CrossRef](#)] [[PubMed](#)]
11. Wang, N.; Xiong, D.; Deng, Y.; Shi, Y.; Wang, K. Mechanically robust superhydrophobic steel surface with anti-icing, uv-durability, and corrosion resistance properties. *Appl. Mater. Interfaces* **2015**, *7*, 6260–6272. [[CrossRef](#)] [[PubMed](#)]
12. Marmur, A. The lotus effect: Superhydrophobicity and metastability. *Langmuir* **2004**, *20*, 3517–3519. [[CrossRef](#)] [[PubMed](#)]
13. Ancona, A.; Joshi, G.S.; Volpe, A.; Scaraggi, M.; Lugarà, P.M.; Carbone, G. Non-uniform laser surface texturing of an un-tapered square pad for tribological applications. *Lubricants* **2017**, *5*, 41. [[CrossRef](#)]
14. Jagdheesh, R.; Diaz, M.; Oca, J.L. Bio inspired self-cleaning ultrahydrophobic aluminium surface by laser processing. *RSC Adv.* **2016**, *6*, 72933–72941. [[CrossRef](#)]
15. Hauschwitz, P.; Jagdheesh, R.; Rostohar, D.; Brajer, J.; Kopeček, J.; Jiříček, P.; Houdková, J.; Mocek, T. Nanostructure fabrication on the top of laser-made micropillars for enhancement of water repellence of aluminium alloy. *Mater. Lett.* **2019**, *256*, 126601. [[CrossRef](#)]
16. Samanta, A.; Wang, Q.; Shaw, S.K.; Ding, H. Nanostructuring of laser textured surface to achieve superhydrophobicity on engineering metal surface. *J. Laser Appl.* **2019**, *31*, 022515. [[CrossRef](#)]
17. Ancona, A.; Carbone, G.; Filippis, M.D.; Volpe, A.; Lugarà, P.M. Femtosecond laser full and partial texturing of steel surfaces to reduce friction in lubricated contact. *Adv. Opt. Technol.* **2014**, *3*, 539–547. [[CrossRef](#)]

18. Sportelli, M.C.; Clemente, M.; Izzi, M.; Volpe, A.; Ancona, A.; Picca, R.A.; Palazzo, G.; Cioffi, N. Exceptionally stable silver nanoparticles synthesized by laser ablation in alcoholic organic solvent. *Colloids Surf. Physicochem. Eng. Asp.* **2018**, *559*, 148–158. [[CrossRef](#)]
19. Gaudiuso, C.; Volpe, A.; Ancona, A. One-step femtosecond laser stealth dicing of quartz. *Micromachines* **2020**, *1*, 327. [[CrossRef](#)]
20. Volpe, A.; Paiè, P.; Ancona, A.; Osellame, R. Polymeric fully inertial lab-on-a-chip with enhanced-throughput sorting capabilities. *Microfluid. Nanofluid.* **2019**, *23*, 37. [[CrossRef](#)]
21. Jagdheesh, R.; Hauschwitz, P.; Mužík, J.; Brajer, J.; Rostohar, D.; Jiříček, P.; Kopeček, J.; Mocek, T. Non-fluorinated superhydrophobic Al7075 aerospace alloy by ps laser processing. *Appl. Surf. Sci.* **2019**, *493*, 287–293. [[CrossRef](#)]
22. Wang, H.; He, M.; Liu, H.; Guan, Y. One-step fabrication of robust superhydrophobic steel surfaces with mechanical durability, thermal stability, and anti-icing function. *ACS Appl. Mater. Interfaces* **2019**, *11*, 25586–25594. [[CrossRef](#)] [[PubMed](#)]
23. Cardoso, J.T.; Aguilar-Morales, A.I.; Alamri, S.; Huerta-Murillo, D.; Cordovilla, F. Superhydrophobicity on hierarchical periodic surface structures fabricated via direct laser writing and direct laser interference patterning on an aluminium alloy. *Opt. Lasers Eng.* **2018**, *111*, 193–200. [[CrossRef](#)]
24. Vercillo, V.; Tonnicchia, S.; Romano, J.; García-girón, A.; Aguilar-Morales, A.I.; Alamri, S.; Dimov, S.S.; Kunze, T. Design rules for laser-treated icephobic metallic surfaces for aeronautic applications. *Adv. Funct. Mater.* **2020**, *30*, 1910268. [[CrossRef](#)]
25. Xing, W.; Li, Z.; Yang, H.; Li, X.; Wang, X.; Li, N. Anti-icing aluminum alloy surface with multi-level micro-nano textures constructed by picosecond laser. *Mater. Des.* **2019**, *183*, 108156. [[CrossRef](#)]
26. Vercillo, V.; Cardoso, J.T.; Huerta-Murillo, D.; Tonnicchia, S.; Laroche, A.; Guillén, J.A.M.; Ocaña, J.L.; Lasagni, A.F.; Bonaccorso, E. Durability of superhydrophobic laser-treated metal surfaces under icing conditions. *Mater. Lett. X* **2019**, *3*, 100021. [[CrossRef](#)]
27. Quéré, D.; Lafuma, A.; Bico, J. Slippery and sticky microtextured solids. *Nanotechnology* **2003**, *14*, 1109–1112.
28. Bizi-Bandoki, P.; Valette, S.; Audouard, E.; Benayoun, S. Time dependency of the hydrophilicity and hydrophobicity of metallic alloys subjected to femtosecond laser irradiations. *Appl. Surf. Sci.* **2013**, *273*, 399–407. [[CrossRef](#)]
29. Cardoso, J.T.; Garcia-Giron, A.; Romano, J.M.; Huerta-Murillo, D.; Jagdheesh, R.; Walker, M.; Dimov, S.S.; Ocaña, J.L. Influence of ambient conditions on the evolution of wettability properties of an IR-, ns-laser textured aluminium alloy. *RSC Adv.* **2017**, *7*, 39617–39627. [[CrossRef](#)]
30. Giannuzzi, G.; Gaudiuso, C.; Mundo, R.D.; Mirengi, L.; Fraggelakis, F.; Kling, R.; Lugarà, M.P.; Ancona, A. Applied surface science short and long term surface chemistry and wetting behaviour of stainless steel with 1D and 2D periodic structures induced by bursts of femtosecond laser pulses. *Appl. Surf. Sci.* **2019**, *494*, 1055–1065. [[CrossRef](#)]
31. Zhang, D.; Chen, F.; Yang, Q.; Yong, J.; Bian, H.; Ou, Y.; Si, J.; Meng, X.; Hou, X. A simple way to achieve pattern-dependent tunable adhesion in superhydrophobic surfaces by a femtosecond laser. *ACS Appl. Mater. Interfaces* **2012**, *4*, 4905–4912. [[CrossRef](#)] [[PubMed](#)]
32. Cassie, A.B.D.; Baxter, S. Wettability of porous surfaces. *Trans. Faraday Soc.* **1944**, *40*, 546–551. [[CrossRef](#)]
33. Jung, S.; Tiwari, M.K.; Doan, N.V.; Poulikakos, D. Mechanism of supercooled droplet freezing on surfaces. *Nat. Commun.* **2012**, *3*, 615. [[CrossRef](#)] [[PubMed](#)]
34. Yin, L.; Wang, Q.; Xue, J.; Ding, J.; Chen, Q. Stability of superhydrophobicity of lotus leaf under extreme humidity. *Chem. Lett.* **2010**, *39*, 816–817. [[CrossRef](#)]
35. Wang, J.; Liu, Z.; Gou, Y.; Zhang, X.; Cheng, S. Deformation of freezing water droplets on a cold copper surface. *Sci. China Ser. E Technol. Sci.* **2006**, *49*, 590–600. [[CrossRef](#)]

